INFLUENCE OF PEG CONFORMATION ON EFFICACY OF SILICA NANOPARTICLE IMMUNOTHERAPY FOR METASTATIC TUMORS

by

WYATT BECICKA

Submitted in partial requirement of the fulfillment for the degree of Master of Science

Thesis Advisor: Dr. Efstathios Karathanasis

Department of Biomedical Engineering

CASE WESTERN RESERVE UNIVERSITY

January 2021

Case Western Reserve University

School of Graduate Studies

We hereby approve the thesis of

Wyatt Becicka

Candidate for the degree of Master of Science

Committee Chair

Dr. Efstathios Karathanasis

Committee Member

Dr. Horst Von Recum

Committee Member

Dr. David Wald

Date of Defense

October 19, 2020

*We also certify that written approval has been obtained for any proprietary material contained therein.

Table of Contents

List of Figures

Figure 4. Evaluation of the microdistribution of immuno-MSN variants with different levels of PEGylation in the tumor immune microenvironment in the orthotopic 4T1 mouse model (page 18). (A) Schedule of administration and analysis of systemically injected fluorescently labeled immuno-MSN particles. **(B)** Flow cytometry analysis showed the high content of resident immune cells in the microenvironment of primary tumor and lung metastasis (top panel) including high levels of the immunosuppressive phenotype of M2-like macrophages (bottom panel). **(C)** Flow cytometry analysis of the uptake of fluorescently labeled immuno-MSN by immune cells, DCs, NK cells and macrophages in the primary tumor and lung metastasis (n=5). **(D)** Flow cytometry analysis of cell uptake of fluorescently labeled immuno-MSNs in blood and spleen (n=5). Statistical significance in the box and whisker plot (5-95 percentile, "+" mean) was conducted by two-way ANOVA with Sidak's post-test (NS not significant, *P<0.05, **P<0.01, ***P<0.001, ****P<0.0001).

Figure 5. Evaluation of the efficacy of the immuno-MSN variants in the orthotopic 4T1 mouse model (page 20). (A) Treatment regimen of immuno-MSN variants at a dose of 10 μg CDN per dose (n=5 mice per group). Quantification of longitudinal BLI imaging is shown for **(B)** primary tumor and **(C)** lung metastasis. **(D)** The size of the primary tumor was measured using a caliper. Flow cytometry analysis of DCs, monocytes and NK cells is shown for **(E)** the primary tumor and **(F)** lungs and blood. Statistical significance in the box and whisker plot (5-95 percentile, "+" mean) was conducted by two-way ANOVA with Sidak's post-test (NS not significant, *P<0.05, **P<0.01, ***P<0.001, ****P<0.0001). Cell count data from flow cytometry analysis was normalized to 10^5 viable cells

Acknowledgments

I would like to acknowledge all of the advice, patience, and support I received throughout the duration of my research at Case Western Reserve University from members of the Stathis lab. I am thankful in particular for the guidance and knowledge passed onto me by my advisor Dr. Karathanasis and soon-to-be professor Dr. Atukorale who was a postdoctoral fellow while I was working in the lab. I am also grateful for the willingness of the greater Case Western community to share ideas and thoughts and provide a supportive environment for one another. Additionally, the excellent resources made available at Case Western for biomedical engineering research is reflective of an administration that is passionate and engaged at all levels.

I also want to acknowledge the support of my family and friends, which became especially valuable during the Covid-19 pandemic this year. They displayed lots of patience and support for me to continue to be productive and motivated during a particularly challenging time. There are many lessons that I have gained during my time at Case Western, from technical skills to personal growth. In the coming years I am excited to pay forward the investment Case Western Reserve University has made in me, and hope to contribute to a socially conscience and involved scientific community.

This work was supported by grants from the National Cancer Institute (U01CA198892), Case Comprehensive Cancer Center GI SPORE 2P50CA150964-07A1, the Case Comprehensive Cancer Center Support Grant (P30CA043703) and the Shiverick Family Fund, the Clinical Translational Science Collaborative of Cleveland (UL1TR002548), and the Alex's Lemonade Stand Foundation. We acknowledge the Case Center for Imaging Research, Case Comprehensive Cancer Center Flow Cytometry Core, and the Case School of Medicine Light Microscopy Core.

List of Abbreviations

BLI	Bioluminescent Imaging
cdGMP	Cyclic Diguanylate Monophosphate
CDN	Cyclic Dinucleotide
CTAB	Cetyltrimethylammonium Bromide
DAMP	Damage-Associated Molecular Pattern
DC	Dendritic Cell
DLS	Dynamic Light Scattering
ELISA	Enzyme-Linked Immunosorbent Assay
FITC	Fluorescein Isothiocyonate
GFP	Green Fluorescent Protein
ICB	Immune Checkpoint Blockade
ICI	Immune Checkpoint Inhibitor
IFN	Interferon
MSN	Mesoporous Silica Nanoparticle
NKC	Natural Killer Cell
NLR	NOD-Like Receptor
PEG	Polyethylene Glycol
PEI	Polyethyleneimine
STING	Stimulator of Interferon Gene
TAM	Tumor Associated Macrophage
TEOS	Tetraethylorthosilicate
TLR-9	Toll-Like Receptor 9

Influence of PEG Conformation on Efficacy of Silica Nanoparticle Immunotherapy for Metastatic Tumors

by

WYATT BECICKA

Abstract

Although the average cancer mortality rate has steadily declined over the past 25 years, the majority of advanced disease remains resistant to current treatment methods and yields dismal prognoses.[1] Novel immunotherapies such as CAR T-cell transfer therapy and ICB provide promising avenues to overcome tumor-mediated immune evasion and initiate an adaptive immune response towards cancer cells. The strongly immunosuppressive microenvironment in advanced tumors, however, can limit the downstream potential of these therapies, and to date these therapies have provided mixed clinical results.[2,3] In an attempt to reverse the immunosuppressive tumor microenvironment, we have designed a MSN that can traffic a STING agonist—cdGMP—into innate immune cells and produce a nearly 9-fold increase in pro-inflammatory IFN-β secretion compared to the free agonist. In a metastatic 4T1 model, the surface density of PEG molecules dictates what innate immune cells have access to systemically injected MSNs. Following treatment with cdGMP-loaded MSNs, this differential distribution and uptake of particles leads to differences in innate immune cell recruitment at metastatic sites and in the blood. It is displayed that an immunostimulatory nanoparticle can be engineered to enhance innate immune cell activation in advanced, metastatic disease, providing a tool that may be able to work in combination with other current immunotherapies to yield more robust and consistent therapeutic responses.

Key words

Cancer immunotherapy, mesoporous silica nanoparticle, systemic drug delivery, STING agonist, PEG

Thesis Overview

Treating advanced cancer faces significant challenges in drug delivery: cancer cell phenotypes exhibit great heterogeneity in between and within patients, the presence of distal colonies of cancer cells limits the efficacy of surgical intervention, and ability to establish resistance makes it challenging to consistently delivery effective doses without incurring significant off-site toxicity. We have attempted to address some of these obstacles in advanced cancer by engineering a MSN with the ability to sequester and deliver immunotherapies to immune cells in the vicinity of cancer cells. This process is discussed in the following five chapters of this thesis.

Chapter 1: Introduction

1.1. Background and Significance

Immunotherapy is a relatively new branch of cancer therapy that seeks to overcome the natural immunosuppressive tumor microenvironment to generate a host immune response against a tumor. While the early clinical successes of immune checkpoint inhibitors and CAR T-cell therapies generated a great deal of excitement, there are a wide variety of cancers that only respond minimally to these treatments.[4] This limited success may be attributed to the fact that many solid tumors are highly immunosuppressive at the time they are diagnosed. These immunologically "cold" tumors have recruited lymphocytes that produce immunosuppressive cytokines, both limiting activation of local innate immune cells and slowing the infiltration of systemic immune cells.[5,6] Without reversing this immunosuppressive microenvironment a tumor will remain immune-privileged, with a strong chemical gradient that dissuades an anti-tumor response from the host immune system.

As tumors develop from "hot" to "cold," they exclude many key immune players to the periphery of the tumor. For instance, perivascular regions become populated with a large concentration of M2-like TAMs, which produce immunosuppressive cues that inactivate nearby immune cells.[6] Among these inactivated cell subsets are dendritic cells that serve as vital antigen presenting cells for creating a functional t-cell response and NKCs that can promote pro-inflammatory signals leading to dendritic cell activation.[7,8,9] As a result, delivery of pro-inflammatory immunoadjuvants into this perivascular immune cell population has the potential to generate a strong pro-inflammatory response, removing the chemical barrier to external immune cell infiltration while enabling innate immune cells to target cancer cells. Systemic administration of nanoparticles

provides convenient access to these innate immune players, with evidence showing that nanoparticles accumulate in the perivascular region of tumors where they are endocytosed into this array of dysfunctional immune cells.[10,11]

In the context of drug delivery, PEG has historically been used on the surface of nanoparticles to evade immunosurveillance.[12] The presence of an inert, hydrophilic polymer on the particle surface sterically hinders non-specific protein adsorption that would otherwise lead to increased immunogenicity of a drug delivery vehicle. For the delivery of adjuvants to immune cells, however, a balance needs to be struck between enhanced immune evasion to avoid off-site uptake and associated toxicity and reduced uptake by target immune cells. In particular, the density of PEG molecules on the surface of a nanoparticle may influence their molecular conformation and thus their immunoevasion behavior.[13] At low densities, PEG molecules take on a mushroom conformation where molecules are free to move independent of one another and effectively fill a hemisphere of space corresponding to the particle's Flory radius; meanwhile, at high densities PEG molecules take on a brush conformation, where molecules restrict one another to exist in a more radially outward configuration. The specific conformation of surface PEG has been shown to influence the destination and extent of target cell uptake for nanoparticles in both in vitro and in vivo experiments.[14,15] Considering the complex network of feedback between immune cells**,** it is important to determine the influence of surface PEG conformation on the distribution and uptake of an immunotherapy nanoparticle into different innate immune cell subtypes.

CDN STING agonists are small molecules that activate our body's natural response to foreign DNA through activation of the STING pathway. The end result of the STING pathway is secretion

of type I IFNs—predominantly IFN-β—that promote a cascade of pro-inflammatory events, including pro-inflammatory t-cell responses, DC maturation, and NKC activation.[16,17] Despite its potent pro-inflammatory potential for cancer immunotherapies, CDN faces a number of challenges in drug delivery. First, it is limited by its high off-site toxicity and undergoes rapid enzymatic degradation in vivo.[17] Further, it is a charged molecule that must cross a hydrophobic cell membrane to activate the STING pathway.

MSNs provide an extremely high specific surface area, enabling a very high active drug-to-excipient ratio.[18] Additionally, the surfaces of MSNs can be readily functionalized with positively charged amines that can tightly bind the negative phosphonate groups in CDN. In order to bypass the cell membrane, it has been shown that particles with a high density of amines with pKa's in the range of 6-7 can disrupt endosomal acidification and cause endosomal lysis via a phenomenon known as the proton sponge effect.[19] As the endosome actively pumps hydrogen ions into the interior of the endosome, basic groups on particles endocytosed by the cell can adsorb these protons and become positive, generating an electrochemical gradient that causes small negative ions to flow into the endosome. In turn, the accumulated ions inside the endosome create an osmotic gradient that causes water to flow into the endosome, causing the compartment to swell and lyse and exposing the nanoparticles to the cell cytoplasm. Ethylene triamine is a small molecule with three amines in close proximity, giving these amines a pKa in the target range of 6-7.[20] By adding a high density of this molecule onto the surface of mesoporous silica, MSNs are not only able to closely bind CDN as they traffic the drug to the perivascular regions of a tumor, but also have potential to bypass the cell membrane to deliver charged STING agonists directly into the cell cytoplasm where they are active.

1.2. Hypothesis and Objectives

The overall objective of this research project was to investigate the effect of surface PEG conformation on the systemic delivery of immunoadjuvant-loaded MSNs to innate immune cells in the vicinity of cancer sites. To this end, first we needed to synthesize and characterize a reproducible MSN with a high density of ethylene triamine. Next, it was necessary to establish stable loading of a CDN immunoadjuvant into the MSN and display increased efficacy of the MSN-CDN formulation compared to free CDN. With the in vitro viability of the formulation confirmed, we then needed to identify the effect of various PEG densities on the microdistribution of particles within cancer sites; specifically, we had to ascertain how PEG conformation effects what immune cells receive the CDN-MSNs in the vicinity of the cancer. Finally, we wanted to show that the differential uptake of particles due to surface PEG density translated into different in vivo outcomes in a metastatic tumor model. To this end, we attempted to mechanistically show that variable particle uptake as a result of PEG conformation effects the ability of the CDN-MSNs to activate and recruit innate immune cells in the vicinity cancer. Based on the known properties of surface PEG coverage, we predicted that more dense PEG surface coverage will exhibit reduced uptake and retention in the innate immune cells populating tumors and metastatic colonies. In turn, this should result in mitigated recruitment and activation of the innate immune cells necessary to counteract the immunosuppressive tumor microenvironment.

Chapter 2: Materials and Methods

2.1. NH_2-MSN Synthesis

5.7 mL of a 25% (wt:wt) aqueous cetyltrimethylammonium bromide (CTAB, Sigma-Aldrich) solution was combined with 14.3 mL of deionized water. The resultant solution was raised to $75°C$ and stirred for 15 minutes. Next, 0.8 mL of freshly prepared 10% aqueous triethylamine (TEA) was added and allowed to stir for 15 minutes. 1.5 mL of the silica precursor tetraethylorthosilicate (TEOS, Sigma-Aldrich) was then added at a rate of 0.1 mL/minute. To generate MSNs in the range of 60 nm, this reaction was allowed to evolve for 1 hour at $80°C$. After 1 hour, the reaction was quenched by diluting in EtOH and the particles were washed several times with EtOH via centrifugation below 5000 rpm. Prior to the removal of CTAB, particles were resuspended in a volume of deionized water corresponding 2 mL of H_2O to 25 mg of MSN for surface functionalization. The pH of the suspension was adjusted with ammonium hydroxide into the range of 8.0 – 9.0, and the particle solution was pre-annealed at $70°C$. 50 uL of [N1-(3-Trimethoxysilylpropyl) diethylenetriamine] (Santa Cruz Biotechnology) was added dropwise and allowed to react for 3 hours before the reaction was quenched in ethanol. For CTAB removal, the particles were washed in a MeOH and HCl solution (500:19, v/v) for 24 hours at room temperature. The particles were collected via centrifugation and thoroughly washed in EtOH.

2.2. MSN Size and Surface Charge Characterization

The size of the MSNs was determined by two methods. First, dilute suspensions of MSNs in EtOH were applied to 3 nm carbon film grids (Ted Pella) and allowed to dry. Next, a FEI Tecnai F30 300 keV Transmission Electron Microscope was used to image the particle samples. TEM images of multiple independently synthesized batches were analyzed in ImageJ to calculate a hard sphere

diameter for the MSNs. The hydrodynamic diameter and surface charge of the particles were measured via dynamic light scattering and electrophoretic light scattering, respectively (90Plus, Brookhaven Instruments).

2.3. CDN-MSN Loading and Release Experiments

To load STING agonist into the particles, MSNs were washed multiple times in water at a pH of 10.2 via repeated sonication and centrifugation. Washed particles were then suspended with cGMP (InvivoGen) in a solution of water at a pH of 10.2 at a ratio of 65 ug cGMP per 1 mg MSN, and the suspension was shaken at room temperature for a minimum of 8 hours. Afterwards, the particles were centrifuged out and cGMP loading was measured via spectrophotometry measurements of the loading supernatant at a wavelength of 284 nm (Tecan Infinite 200). For stability studies, CDN-MSNs were suspended in PBS at $37°C$ (pH of 5.5 or 7.4), and cGMP release was measured across a 20k MWCO mini dialysis unit (Thermo Fisher Scientific) at regular intervals.

2.4. Cells and Animal Models

Metastatic murine 4T1 breast adenocarcinoma cells expressing green fluorescent protein and luciferase (gifted from the Jeremy Rich Lab at USCD) and murine RAW 264.7 macrophages (ATCC) were cultured in DMEM (Gibco) containing 10% FBS (Hyclone) and 1% penicillin-streptomycin (Sigma-Aldrich). Short tandem repeat analysis was used to validate all cell lines and regular testing was performed for Mycoplasma contamination. Cells were cultured at $37°C$ and 5% CO_2.

To generate an orthotopic 4T1 model, female C57BL/6 albino mice (Jackson Laboratories) between 8-10 weeks were anaesthetized, shaved, and a 1-2 mm incision was made in the lower left abdomen. 5×10^5 4T1 cells were injected into the mammary fat pad in ___ μL of PBS. After inoculation, mice were monitored daily until a palpable tumor was confirmed, at which point tumor progression was monitored via tumor caliper measurements (longest axis and perpendicular width) and bioluminescent imaging (IVIS Spectrum, Perkin Elmer) 10 minutes after intraperitoneal injection of 200 μL of D-luciferin at 12.5 mg/mL. In all in vivo studies, mice were treated with their first particle dose on day 8, and in treatment studies this was followed with a second treatment on day 9.

2.5. In Vitro Analysis of MSN-CDN Efficacy

To measure the buffering capacity of the NH_2-MSNs, the particles were suspended in a deionized water and NH_4OH was added dropwise to achieve a pH above 9. Next, 1M HCl was added in 1 μL increments and the subsequent pH of the solution was recorded. The buffering capacity was then calculated as the change in pH per μL of 1M HCl added.

Next, the intracellular distribution of particles as a function of time was qualitatively investigated. To visualize particles, NH_2-MSNs were reacted with an Alexa 546 NHS dye (200:1, wt/wt) in deionized water for 2 hours. RAW 264.7 macrophages (300,000 cells/mL) were allowed to adhere to a glass bottom cell culture dish for 24 hours before they were treated with the AF647-MSNs at 0.72 mg MSN/mL. Samples were collected 2 and 6 hours following treatment, rapidly washed with PBS, fixed with 2% PFA in PBS for 30 minutes, and then mounted onto a glass slide with DAPI mounting medium (Vector Laboratories) onto No. 1.5 glass cover slips. Confocal images of

the particles and cells were captured with a TCS SP8 gated STED confocal microscope (Leica Microsystems).

To determine that enhanced intracellular distribution of the immuno-MSN corresponded to increased therapeutic efficacy, the IFN-β production of RAW 2647 macrophages exposed to CDN-MSNs and free CDN was compared. 6 million RAW 2647 macrophages were co-plated in 1.5 mL of cell media with treatments of 30 μg of free CDN and MSN-loaded CDN. After 24 hours, the media was spun at cell speed and the supernatant collected. mIFN-β production was measured following the manufacturer's protocol using a LumiKine Xpress Bioluminescent Cytokine ELISA Kits (InvivoGen) and luminescence readings were obtained with the Tecan Infinite 200 spectrophotometer.

2.6. Generation of Different PEG Conformations

NH_2-MSNs were suspended in deionized water at 10 mg/mL and pH was adjusted to near neutral (7.0-7.5). 2 kDa NHS-PEG-FITC (NANOCS) was dissolved in DMSO and added to the particle suspension at ratios varying from 2:1 to 200:1 (wt:wt). The suspension was reacted on a shaker for 2 hours at room temperature. Once the reaction was complete, the reaction supernatant was collected and absorption was read at 494 nm (Tecan Infinite 200) to measure. the amount of PEG-FITC reacted to the surface of the MSN. For flow cytometry experiments, 2KDa mPEG-NHS succinic acid (NANOCS) was used in place of FITC-PEG-NHS. The zeta potential of each particle formulation was measured (90Plus, Brookhaven Instruments) to ensure a positive surface charge had been retained.

2.7. Institutional Animal Care and Use Committee Statement

All animal procedures were conducted under protocols approved by the Institutional Animal Care and Use Committee (IACUC) of Case Western Reserve University.

2.8. NH_2-MSN Biodistribution and Treatment FACS Studies

DAPI, CD45 (30-F11), CD3e (145-2C11), CD11b (M1/70), CD11c (HL3), CD19 (1D3), CD49b (DX5), and F4/80 (T45-2342) dye-conjugated flow cytometry antibodies were purchased from BD Biosciences. Anti-mouse CD4 (GK1.5), CD8a (53-6.7), CD25 (3C7), CD80 (16-10A1), CD206 (C068C2), Ly-6C (HK1.5), and Ly-6G (1A8) antibodies were purchased from Biolegend.

To analyze biodistribution, AlexaFluor 750 NHS (Thermo Fisher Scientific) was reacted with densely PEGylated, lightly PEGylated, and naked NH_2-MSNs for 2 hours in deionized water at room temperature (100:2.15, wt:wt). Three groups of mice (n = 5) orthotopically inoculated with metastatic 4T1 mammary fat pad tumors. On day 8, each group received a single tail vein injection of 0.2 mg of the different NH_2-MSN formulations, and 24 hours later the mice were sacrificed and their spleen, lungs, tumor, and blood collected for FACS analysis. The tumor and lungs were digested in collagenase solution (1 mg/mL, Sigma-Aldrich) and then all organs were homogenized and passed through 70 μm filters. ACK lysis buffer was used to eliminate any remaining red blood cells in the blood and organ cell suspensions. After staining and fixing, cells were read on a BD FACS LSR II Flow Cytometer (Becton Dickinson) and then analyzed with FlowJo software.

For treatment studies, lightly and densely PEGylated NH_2-MSNs were synthesized and loaded with 50 ug CDN / mg MSN. Three groups of n = 5 mice were inoculated with orthotopic 4T1

tumors and separated into two groups treatment groups and an untreated control. On days 8 and 9, the treatment groups received a tail vein injection of either the light or dense CDN-MSN formulation containing 10 ug of CDN. On day 11 organs were collected and FACS analysis was performed.

2.9. Statistical Analysis

Prism 8 software was used for statistical analysis (GraphPad). The statistical methods used included unpaired t-test (two tailed) and one-way ANOVA with Kramer-Tukey post-hoc analysis. All statistical significances reported are for p values of less than 0.05. All groups used in this study included a minimum of 3 biological replicates or, for animal studies, at least 5 mice.

Chapter 3: Results

Partially reproduced from original manuscript submitted to the journal Advanced Healthcare Material that is currently under review, September 2020.

The potential use of CDN STING agonists for cancer therapy faces several daunting barriers. First, CDN faces a challenging therapeutic profile, where its off-site toxicity and rapid enzymatic degradation in vivo limits the ability to achieve sustained doses to target cancer sites. Next, once delivered into the vicinity of the cancer, CDN must reach the desired subset of innate immune cells in a high concentration. As a molecule with multiple charges, CDN also faces the additional challenge of entering the cellular cytoplasm, where it must be present to activate the STING pathway. Cumulatively, we sought to investigate how a silicate nanoparticle could be engineered to overcome these obstacles to CDN drug delivery.

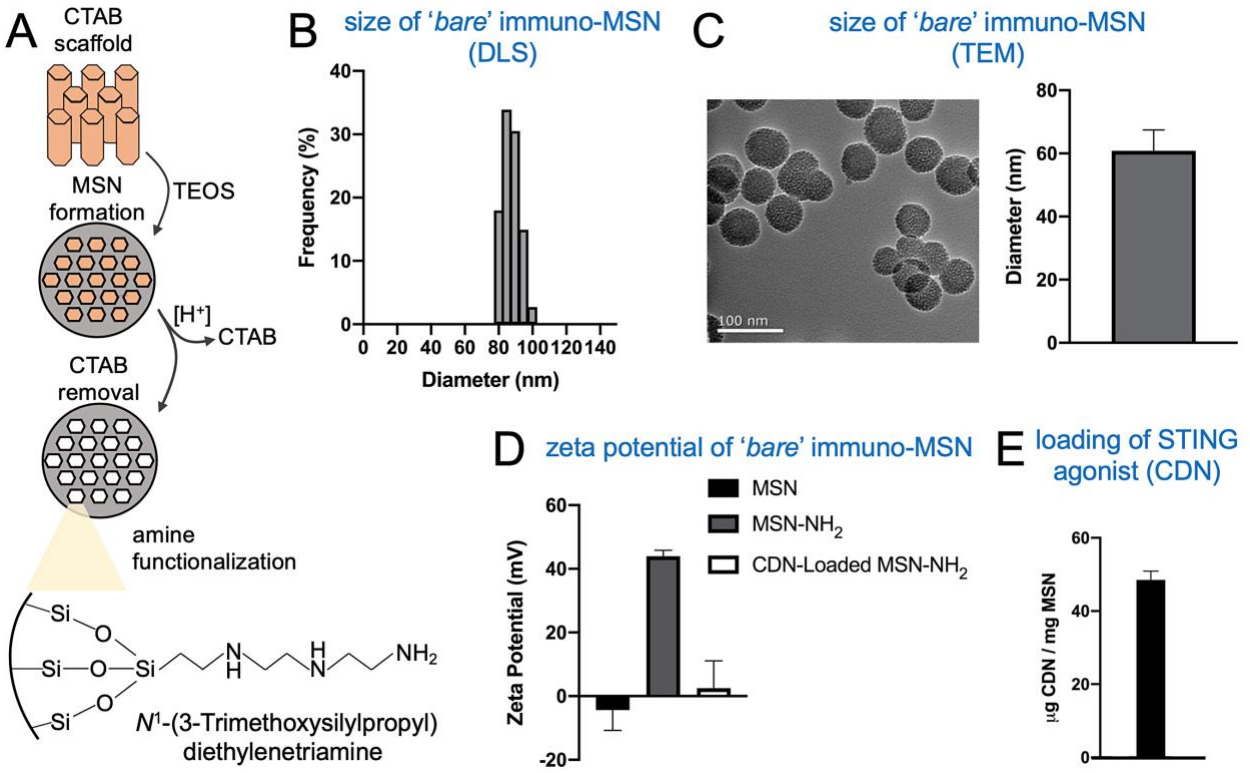

Figure 1. Synthesis of immuno-MSN. (A) Schematic shows the synthesis of the amine-functionalized MSN. **(B)** The hydrodynamic size of MSNs was measured using dynamic light scattering. **(C)** TEM was used to characterize the structure and size of the MSNs. **(D)** The zeta potential of MSNs was measured before and after amine functionalization and after CDN loading. **(E)** Loading of MSN was highly consistent and efficient.

3.1. Synthesis of a NH_2-Mesoporous Silica Nanoparticle

MSNs were elected for our model drug delivery vehicle because they can be engineered to have high surface area (allowing for a large active drug to excipient ratio) and their surface chemistry can be readily modified to stably load a variety of drug molecules. To this end, TEOS underwent a controlled condensation reaction in the presence of a regular hexagonal CTAB scaffold. After the removal of CTAB, this produced a bare MSN that DLS measurements showed to be monodisperse with a hydrodynamic diameter in the range of 80-100 nm (figure 1B). TEM images were also obtained to calculate a uniform hard sphere diameter of 61 ± 6 nm (figure 1 C). In order to create a particle with the ability to tightly bind and sequester CDN from systemic uptake and

degradation, the silica particles were reacted with N^1-(3-Trimethoxysilylpropyl)diethylenetriamine, adding positive diethylenetriamine groups to the surface of the particle that can form an ionic bond with the phosphonate backbone of CDN molecules. Zeta potential measurements of the MSNs before and after this reaction supported the addition of a positive functional group, with zeta potential of the particles rising from -4 ± 6 mV to 44 ± 2 mV (figure 1D). In turn, the ability to load CDN into the MSNs was measured. After known amounts of CDN were added to a suspension of amine-functionalized MSNs, the particles were allowed to react overnight, and then collected via centrifugation. It was observed that 50 ug of CDN / mg of MSN was consistently loaded and thus eliminated from the reaction mixture, as measured by the absorption of light at 284 nm (figure 1E). The loading CDN, and subsequent neutralization of positive amines on the surface of the particle, was also supported the drop of the MSN zeta potential to a near-neutral value of 2 ± 8 mV following loading (figure 1D).

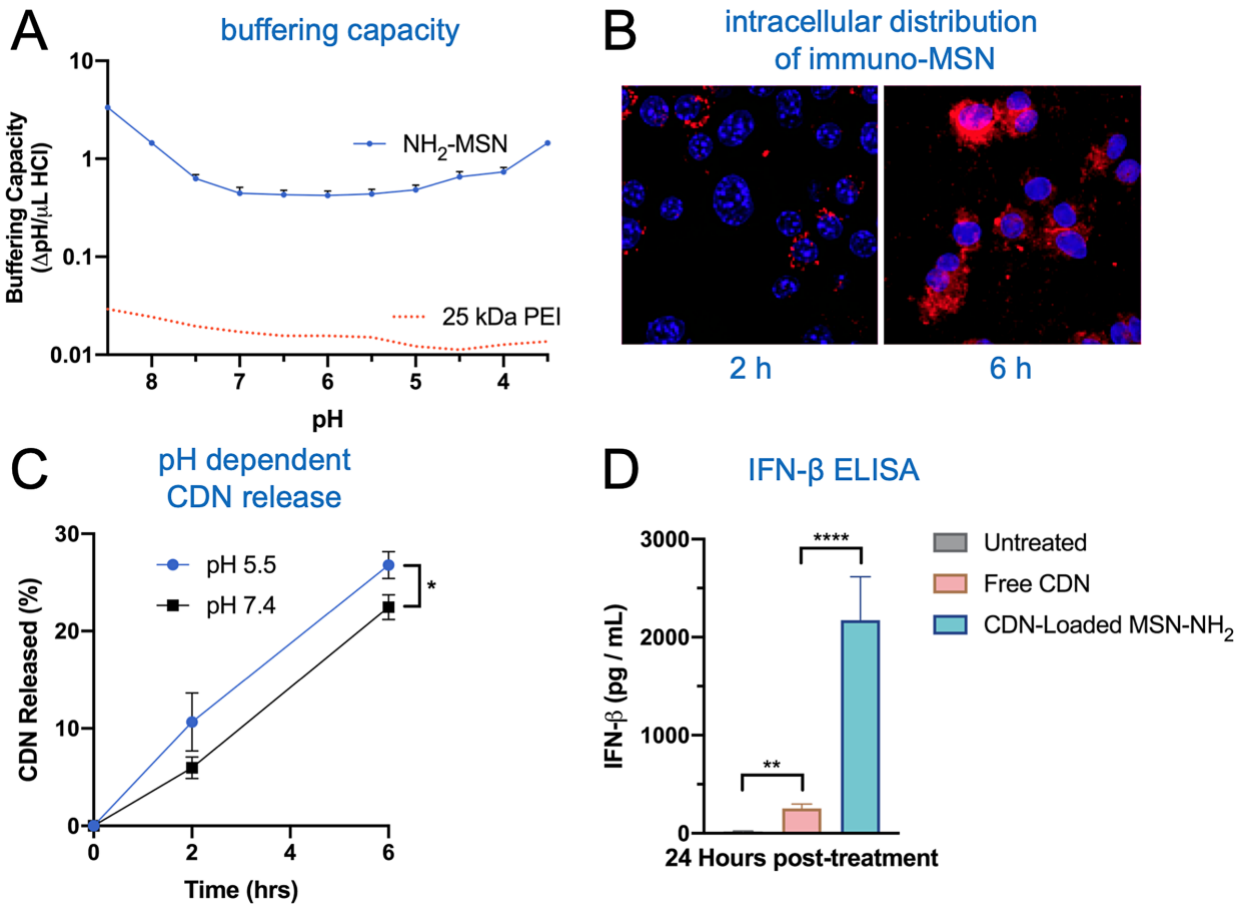

Figure 2. Evaluation of the efficacy of immuno-MSN *in vitro*. (A) Proton buffering of the immuno-NP based on titration curves (n=3). The curve of PEI (red dotted line) was extracted from Benjaminsen et al., 2013. **(B)** Confocal microscopy monitored the intracellular distribution of fluorescently labeled immuno-MSN as a function of time. **(C)** Release of CDN from immuno-MSN at 37°C as a function of pH. **(D)** ELISA analysis measured the *in vitro* production of IFNβ from RAW 264.7 macrophages 24 h after co-incubation with free CDN or immuno-MSN. All conditions were performed in triplicate and plotted as mean ± standard error with statistics by 2-way ANOVA with Tukey's/Sidak's post-test (P values: **<0.01, **** P<0.0001).

3.2. In Vitro Analysis of CDN-MSN Efficacy

In addition to giving the particles a positive charge for loading CDN, diethylenetriamine was selected decorate the MSN because its high number of amines in close proximity provides a strong buffering effect. With an adequately high buffering capacity, particles internalized via endocytosis can manipulate the endosomal acidification process to create a strong osmotic gradient that drives water into the endosome and permeabilizes or lyses an endosome. This mechanism, referred to as the proton sponge effect (citation) provides a potential pathway to bypass the cell membrane and

deliver a highly charged molecule such as CDN into the cytoplasm, where it must be present to stimulate the STING pathway.

To determine if the buffering effect of our particles was in the range necessary to incur a proton sponge effect, we measured the buffering capacity of our particles and normalized this value per particle. Next, we identified 25 kDa PEI as a particle that has been documented to cause the proton sponge effect (citation) and plotted reported values for the buffering capacity of PEI on a par particle basis. In the relevant range of pH from 7.5 to 5.5, we observed that the NH_2-MSNs produced at least an order of magnitude greater buffering capacity per particle than 25 kDa PEI (figure 2A). Next, to support that the high buffering capacity of NH_2-MSNs resulted in endosomal escape, confocal images of intracellular particle distribution were captured as a function of time. Unloaded particles were fluorescently labeled and incubated with macrophages, with cells collected, fixed, and stained with DAPI at 2 and 6 hours. While the images at 2 hours showed fluorescent particles were almost exclusively confined to punctate intracellular compartments, images at 6 hours showed fluorescent particles had become diffuse within the cell (figure 2B). In addition to cytoplasmic access, we investigated if the CDN itself would be able to release from the NH_2-MSNs sufficiently under the acidic endosomal conditions. To this end, MSN-loaded CDNs were dialyzed in PBS at $37°C$ at both pH 7.4 (mimicking biological conditions) and pH 5.5 (mimicking late endosomal conditions), and released CDN was measured in the dialysate. It was observed that CDN underwent a small increase in release upon mild acidification (figure 2C). Finally, the effect of NH_2-MSN buffering capacity and endosomal escape on the ability of CDN to generate IFN-β was measured. For this, macrophages were treated with equivalent doses of free CDN and CDN loaded into MSNs and incubated for 24 hours. After treatment, cell-free media was

isolated via centrifugation and IFN-β production was measured with an ELISA. It was observed that the CDN-loaded MSN generated 2200 $\pm$ 400 pg IFN-β/mL compared to 250 $\pm$ 40 pg IFN-β/mL for the free CDN control, representing an increase in CDN efficacy of approximately 9 times (figure 2D).

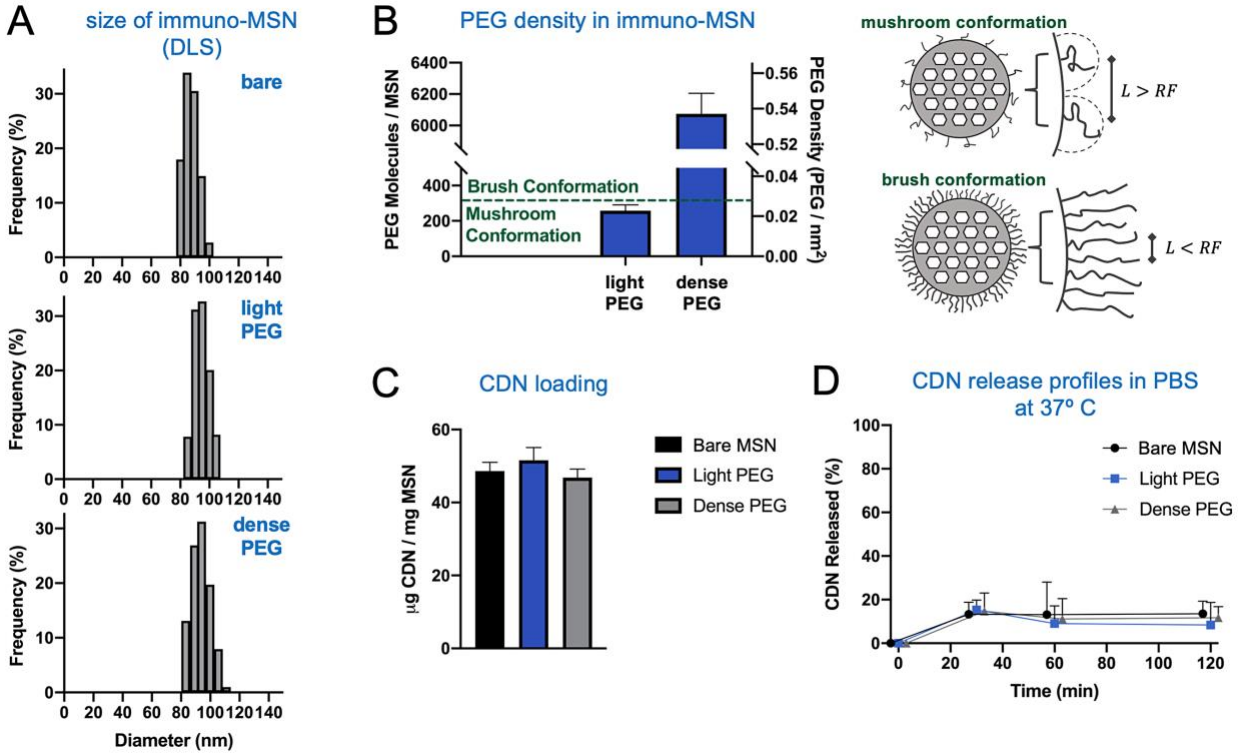

Figure 3. Characterization of immuno-MSN variants with different PEGylation *in vitro*. (A) The hydrodynamic size of the immuno-MSN variants was measured using dynamic light scattering. (**B**) Using fluorescent analysis, the number of PEG molecules per MSN particle was measured. **(C)** The CDN cargo of the immuno-MSN variants is shown. **(D)** Release of CDN from the immuno-MSN variants was evaluated at 37°C.

3.3. Synthesis of CDN-MSNs with different PEG conformations

To optimize the delivery of the CDN-MSN formulation to innate immune cells in the vicinity of the tumor, the impact of PEG molecule conformation on the particle surface was investigated. In particular, it was desired to investigate particles coated with PEG in a mushroom conformation—where PEG molecules are free to move about a hemisphere corresponding to the PEG molecules

Flory radius—and in a brush conformation—where adjacent PEG molecules are close enough to impede one another's motion, confining them to extend radially outward. For the 2 kDa mPEG used in this study, PEG exists in the mushroom conformation below 0.027 PEG molecules/nm^2.[14] To create MSN formulations with these specific surface densities of PEG, varying amounts of NHS-PEG-FITC was reacted with NH_2-MSNs. After the reaction, the particles were isolated via centrifugation and the absorbance of the supernatant at 494 nm was used to determine the amount of PEG-FITC reacted to the surface of the particles. Experimental conditions were determined to add adequate PEG to generate mushroom and a brush conformations, and the DLS measurements for particles before and after PEGylation showed a small increased in diameter (figure 3A,B). CDN loading for the two PEGylated formulations was determined to be consistent with the bare NH_2-MSN and release profiles displayed that all formulations stably loaded more than 80% of CDN for 2 hours.

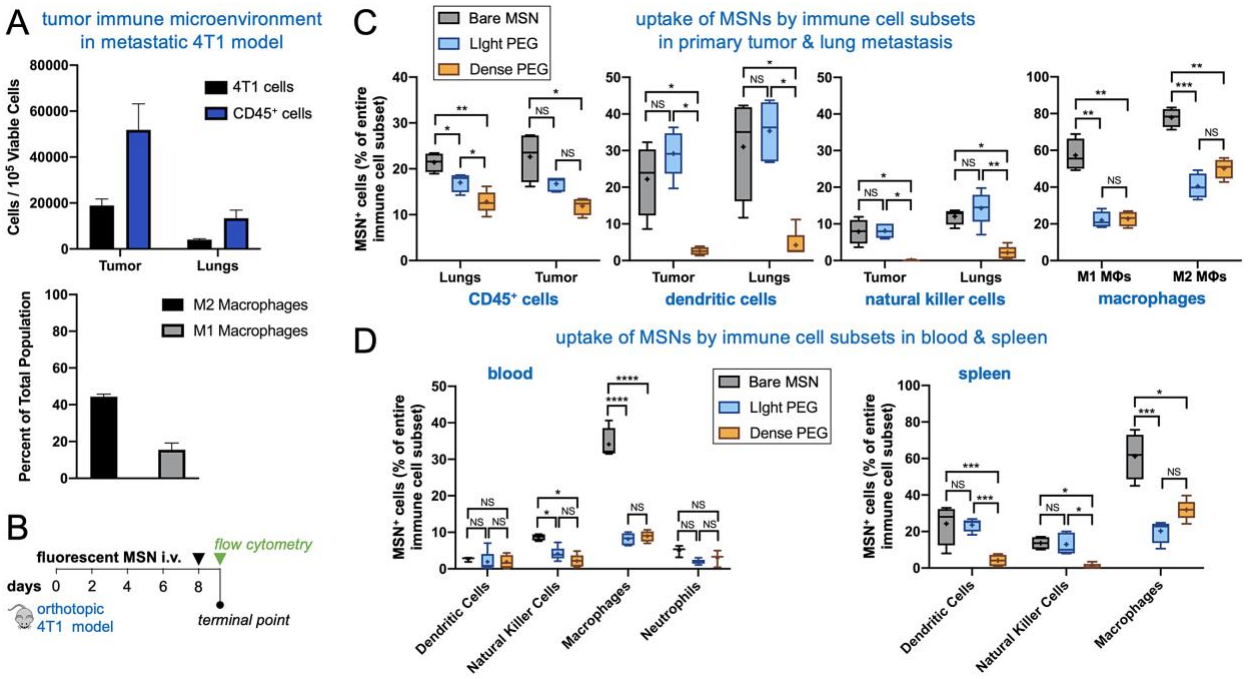

Figure 4. Evaluation of the microdistribution of immuno-MSN variants with different levels of PEGylation in the tumor immune microenvironment in the orthotopic 4T1 mouse model. (**A**) Schedule of administration and analysis of systemically injected fluorescently labeled immuno-MSN particles. (**B**) Flow cytometry analysis showed the high content of resident immune cells in the microenvironment of primary tumor and lung metastasis (top panel)

including high levels of the immunosuppressive phenotype of M2-like macrophages (bottom panel). (**C**) Flow cytometry analysis of the uptake of fluorescently labeled immuno-MSN by immune cells, DCs, NK cells and macrophages in the primary tumor and lung metastasis (n=5). (**D**) Flow cytometry analysis of cell uptake of fluorescently labeled immuno-MSNs in blood and spleen (n=5). Statistical significance in the box and whisker plot (5-95 percentile, "+" mean) was conducted by two-way ANOVA with Sidak's post-test (NS not significant, *P<0.05, **P<0.01, ***P<0.001, ****P<0.0001).

3.4. Effect of PEG Conformation on Innate Immune Cell Uptake of CDN-MSN

To investigate the impact of PEG conformation on the the biodistribution of the CDN-MSN, three groups of five mice received orthotopic 4T1 cell innoculations of 500,000 cells expressing firefly luciferase and GFP. Tumor progress was monitored using BLI until acceptable tumor burden was observed on day 8, when mice in the three groups were treated with 0.2 mg of unloaded bare, lightly PEGylated, or densely PEGylated MSNs that had been fluorescently labeled with AlexaFluor 647. 24 hours later, the mice were sacrificed and the tumor, blood, spleen, and lungs were collected for FACS analysis (figure 4B). To confirm the presence of the desired tumor model, the presence of GFP+ cancer cells were identified in the primary tumors and as metastases in the lungs. To further ensure that the tumor microenvironment was immunosuppressive at this stage, the fraction of M2 and M1 polarized macrophages in the tumor was measured and found to be 44 $\pm$ 1% and 16$\pm$ 4%, respectively (figure 4A).

Next, innate immune cells were isolated via flow cytometry and the fraction of MSN-AF647^{+} cells was identified for each immune cell subset. In total, DCs ($CD45^{+}\rightarrow CD11c^{+}$), NKCs ($CD45^{+}\rightarrow CD49b^{+}$), M1 macrophages/M2 macrophages ($CD45^{+}\rightarrow CD11b^{+}\rightarrow F4/80^{+}\rightarrow CD80^{+}/CD206^{+}$), general immune cells ($CD45^{+}$), and—in the blood—neutrophils ($CD45^{+}\rightarrow CD11b^{+}\rightarrow Ly6G^{+}\rightarrow Ly6C^{-}$) were analyzed. In the lungs and tumor, the bare MSN was found in a greater fraction of immune cells and both M1 and M2 macrophages, while the light PEG MSN had significantly higher uptake into immune cells in the lungs compared

to the dense PEG MSN. Interestingly, both the bare and light PEG MSNs were endocytosed at similar rates into NKCs and DCs, and both were present in a significantly higher fraction of these cells than the dense PEG MSN (figure 4C). Unsurprisingly, the bare MSN displayed significantly greater uptake in the reticuloendothelial system, appearing in 61 $\pm$ 13% of macrophages in the spleen. Additionally, neither the light nor dense PEG MSN appeared in any immune cells in the blood at greater than 9%, while the bare MSN was present in 9.1 $\pm$ 0.5% and 34 $\pm$ 4% of systemic natural killer cells and macrophages, respectively (figure 4D).

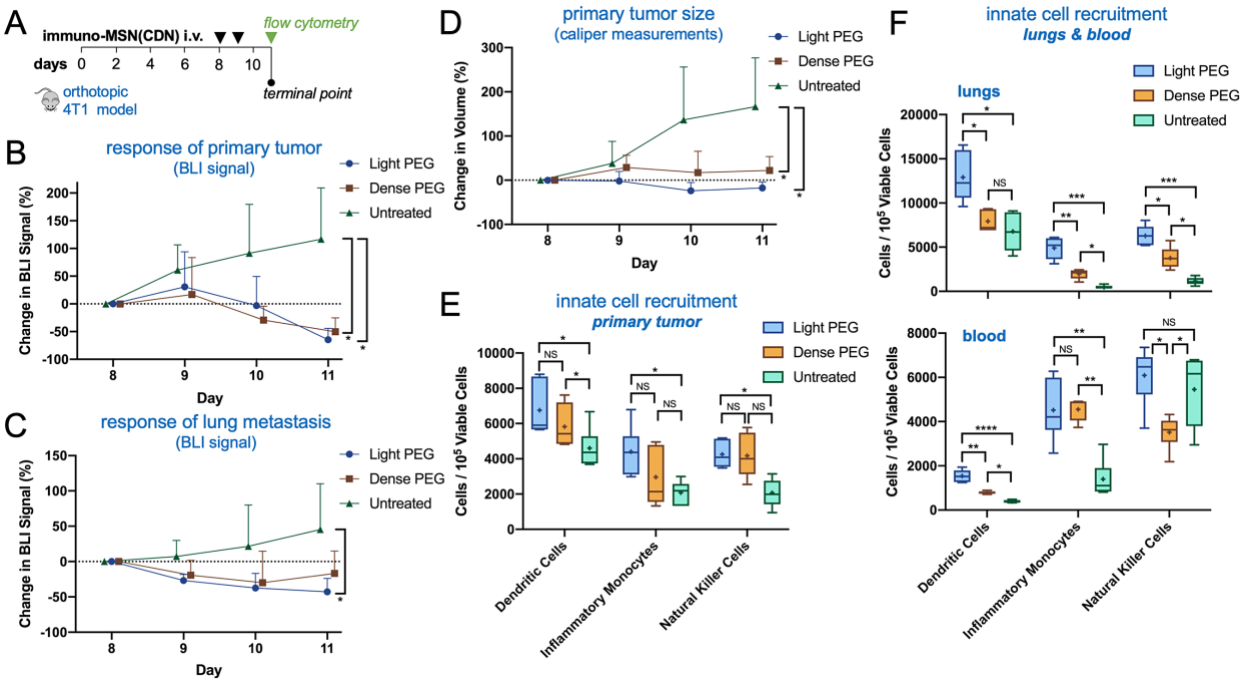

Figure 5. Evaluation of the efficacy of the immuno-MSN variants in the orthotopic 4T1 mouse model. (A) Treatment regimen of immuno-MSN variants at a dose of 10 μg CDN per dose (n=5 mice per group). Quantification of longitudinal BLI imaging is shown for **(B)** primary tumor and **(C)** lung metastasis. **(D)** The size of the primary tumor was measured using a caliper. Flow cytometry analysis of DCs, monocytes and NK cells is shown for **(E)** the primary tumor and **(F)** lungs and blood. Statistical significance in the box and whisker plot (5-95 percentile, "+" mean) was conducted by two-way ANOVA with Sidak's post-test (NS not significant, **P*<0.05, ***P*<0.01, ****P*<0.001, *****P*<0.0001). Cell count data from flow cytometry analysis was normalized to 10^5 viable cells.

3.5. Impact of PEG conformation on Innate Immune Cell Recruitment from CDN-MSNs

To identify the impact of PEG conformation on the efficacy of CDN-MSNs for tumor therapy, a mechanistic study of innate immune cell recruitment was performed. To this end, three groups of five mice received orthotopic inoculations of 500,000 4T1 cancer cells. Two groups of mice were treated on days 8 and 9 with 10 μg of CDN loaded into both the light and dense PEG formulations, while the third group was kept as an untreated control (figure 5A). Compared to the untreated control, both CDN-MSN formulations managed to produce significant reductions in primary tumor BLI signal, primary tumor volume, and metastatic BLI signal (figure 5B,C,D). All groups were sacrificed on day 11 and their tumor, lungs, and blood collected for FACS analysis. In addition to the innate immune populations analyzed in the uptake study, the presence of inflammatory monocytes ($CD45^+ \rightarrow CD11b^+ \rightarrow Ly6C^+ \rightarrow Ly6G^-$) was measured as an indicator of a pro-inflammatory response. In the primary tumor, both PEG formulations generated a significantly greater number of dendritic cells compared to the untreated control, while the light PEG formulation was the only formulation to recruit a significantly greater population of inflammatory monocytes to the tumor microenvironment (figure 5E). Meanwhile, the light PEG formulation produced significantly larger amounts of DCs, inflammatory monocytes and NKCs compared to either of the other groups. Additionally, while both light and dense PEG formulations produced similar amounts of inflammatory monocytes in the blood, the light PEG formulation generated significantly circulating dendritic cells at 1540 ± 280 cells/10^5 viable cells, versus 780 ± 70 cells/10^5 viable cells in the dense PEG scenario.

Chapter 4: Discussion

It is increasingly apparent that the host immune response plays a vital role in the outcome of cancers, with a high density of infiltrating T-cells correlating with improved cancer prognosis.[21] As a result, many clinical immunotherapies are currently focused on harnessing a functional T-cell response, including ICIs and CAR T-cell therapy. Although these therapies have shown promise in treating some cancers, their success has been inconsistent and limited in many advanced diseases.[5] Importantly, advanced tumors contain a high concentration of pro-tumor lymphocytes secreting immunosuppressive cytokines, creating a chemical barrier to systemic T-cell infiltration.[22] Further, while ICIs prevent specific inhibitory T-cell pathways, cancers often respond to ICI treatment by upregulating other pathways that disrupt T-cell function and may develop resistance to ICIs with repeated use.[23] Although the clinical potential of these immunotherapies is clear, it also appears increasingly necessary to supplement these T-cell centric therapies with additional immunoadjuvants to assist in remodeling the immunosuppressive microenvironment of advanced tumors.

STING agonist induces innate immune cells in the tumor microenvironment to secrete IFN-β, and thus has the potential to drive a robust anti-cancer immune response. Locally, IFN-β secretion activates NKCs which can then directly kill tumor cells while activating and recruiting DCs in the tumor microenvironment.[24,25] IFN-β also directly promotes DC maturation, where mature cDC1s secrete cytokines that recruit NKCs to the site of the tumor, creating a potent, self-perpetuating inflammatory immune response.[26] Once mature DCs are exposed to tumor antigens, they migrate to lymph nodes where they can educate a functional t-cell response. Meanwhile, DCs in the tumor microenvironment produce cytokines that are vital for activated t-cells to infiltrate and attack the

tumor.[27] The potential of STING agonists, however, faces several logistical challenges, with one vital challenge including crossing the hydrophobic cell membrane. In our study we found that silica nanoparticles offer great chemical flexibility to not only stably load immunoadjuvants based on charge, but also to imbue the particle with chemical properties—such as a strong buffering capacity—that can enhance cytoplasmic delivery and subsequent IFN-β secretion. Further, utilizing particles designed to achieve endosomal escape has the potential to build potent combination therapies by adding other immunoadjuvants active in the cytosol (NLRs) and interior of the endosome (TLR-9).[28,29,30]

Although effective in vitro, delivery to the desired innate immune cells is another hurdle for cdGMP STING agonists. In vivo, cdGMP undergoes rapid enzymatic degradation and exhibits a high level of off-site toxicity that limits dosing.[17] Although intratumoral administration of immunoadjuvants offers a tempting solution to the issue of local delivery, it is also dependent on tumor accessibility and carries the risk of altering a tumor's internal pressure and physical integrity. Previously, our lab has found that that systemically administered silica nanoparticles deposit in the perivascular region of various murine tumor models, providing access to the numerous inactive innate immune cells present in this space.[31,32,33] To optimize cancer immunotherapy, next generation therapies should not only deliver immunoadjuvants to the site of cancer, but also consider the number and type of different immune cells receiving treatment. In this study, we observed that different surface densities of PEG altered the destination of systemically administered MSNs. Compared to densely PEGylated MSNs, lightly PEGylated MSNs displayed increased uptake into DCs and NKCs in cancer-bearing organs while showing similarly low uptake in off-site macrophages compared to the naked particle. The enhanced

inflammation and recruitment of innate immune cells in mice treated with the lightly PEGylated cdGMP-MSNs—especially for metastases in the lungs—indicates that this altered distribution has an effect on the pro-inflammatory effect of the immunoadjuvant.

This study highlights both the challenges and potential of drug delivery for cancer immunotherapy. The inherent complexity of the immune system and its network of signaling pathways can make it challenging to reproducibly elicit a desired response and even minute changes to a drug delivery system can have a significant impact on the balance of immune cells receiving a treatment and the outcome of a therapy. Meanwhile, this same ability to alter the destination of immunotherapies provides an opportunity to control the types of cells that receive a treatment. In our study, we observed that more densely PEGylated MSNs experience reduced uptake into tumor DCs and NKCs while still accumulating in macrophages at a high rate, which could be desirable for a therapy targeted specifically at macrophages. As the field of drug delivery for cancer immunotherapy continues to grow, it will be important to both understand the influence of surface chemistry on the destination of drug delivery vehicles and combine this information with an in-depth knowledge of cancer immunology to optimize therapeutic efficacy.

Chapter 5: Conclusions and Future Directions

This study displayed that immuno-MSNs can be engineered to stably load negatively charged STING agonists and deliver these across the cell membrane, increasing the efficacy of MSN-loaded CDN nearly 9 times compared to the same dose of administered free CDN. Further, it was determined that PEG conformation influences the destination of fluorescently-labeled MSNs in vivo, with MSNs presenting a low-density mushroom conformation exhibiting greater uptake into innate immune cells in the vicinity of cancer compared to MSNs covered in a dense brush conformation. Independent of PEGylation, both CDN-MSN formulations displayed significant short-term therapeutic effects after only two intravenous treatments of 10 ug CDN per mouse. A mechanistic study of innate immune cell recruitment, however, indicated that the enhanced uptake of lightly PEGylated MSNs compared to the densely PEGylated formulation increased recruitment of immune cells to metastases in the lungs and produced nearly twice as many circulating dendritic cells, necessary for educating a t-cell response in the lymph nodes. The trends observed display that subtle factors such as the conformation of PEG on the surface of a nanoparticle can drastically alter the types and number of cells receiving systemic therapies, and should be considered when testing novel drug delivery systems for immunotherapies.

As many current studies have identified the necessity for combinatorial immunotherapy treatments to maximize efficacy, this drug delivery system should be investigated in combination with other pro-inflammatory drugs. In particular, TLR-9 agonists that can induce TAMs to repolarize to a pro-inflammatory M1 phenotype could be investigated as a potential syngeneic therapy. Moving forward, it may be desirable to target CDN-MSN formulations to various markers upregulated at metastatic sites and in the primary tumor. Since tumors vary both as a function of space and time,

different targeting schemes may enhance treatments for early and late stage cancers. In addition to proper pro-inflammatory immune signals, DAMPs are essential in the process of activating various immune cells, including dendritic cells. Prior to immunotherapy, treatment of tumors with targeted chemotherapy may have the potential to both increase the permeability of the primary tumor to particle penetration and produce large concentrations of DAMPs that should cumulatively enhance a systemic immunotherapy. A variety of chemotherapeutics can be readily loaded into properly functionalized MSNs, and combination therapies of chemotherapy and immunoadjuvants could be tested using the MSN platform. To further refine the design of the CDN-MSN, in the future it may be possible to use late endosome triggers such as pH or the reductive intracellular environment to promote drug release concurrent with the vehicle's entrance into the cell cytoplasm. By using acid-labile or disulfide linkages to tether the positive diethyl triamine groups to the surface of the particle, it may be possible to engineer the particle to strategically release its cargo as it is exposed to the cell cytoplasm, further enhancing the effective dose of loaded drug.

Bibliography

1. Siegel R, Miller K, Jemal A. Cancer statistics, 2020. *Ca Cancer J Clin*. 2020; 70(1): 7-30. doi: 10.3322/caac.21332

2. Ma S, Li X, Wang X, et al. Current Progress in CAR-T Cell Therapy for Solid Tumors. *Int J Biol Sci.* 2019; 15(12): 2548-2560. doi: 10.7150/ijbs.34213

3. Darvin P, Toor S, Nair V, et al. Immune checkpoint inhibitors: recent progress and potential biomarkers. *Exp Mol Med.* 2018; 50(12): 1-11. doi: 10.1038/s12276-018-0191-1

4. Esfahani K, Roudaia L, Miller WH. A review of cancer immunotherapy: from the past, to the present, to the future. *Curr Oncol.* 2020; 27(Suppl 2): S87-S97. doi: 10.3747/co.27.5223

5. Bonaventura P, Shekarian T, Alcazar V, et al. Cold Tumors: A Therapeutic Challenge for Immunotherapy. *Front Immunol.* 2019; 10: 168. doi: 10.3389/fimmu.2019.00168

6. Beatty G, Gladney W. Immune Escape Mechanisms as a Guide for Cancer Immunotherapy. *Clin Cancer Res.* 2015; 21(4): 687-692. doi: 10.1158/1078-0432.CCR-14-1860

7. Lewis C, Harney A, Pollard J. The Multifaceted Role of Perivascular Macrophages in Tumors. *Cancer Cell*. 2016; 30(2): 365. doi: 10.1016/j.ccell.2016.07.009

8. Gardner A, Ruffell B. Dendritic Cells and Cancer Immunity. *Trends Immunol.* 2016; 37(12): 885-865. doi: 10.1016/j.it.2016.09.006

9. Larsen S, Gao Y, Basse P. NK Cells in the Tumor Microenvironment. *Crit Rev Oncog.* 2014; 19(0): 91-105. doi: 10.1615/critrevoncog.2014011142

10. Goldberg M. Improving cancer immunotherapy through nanotechnology. *Nat Rev Cancer.* 2019; 19: 587-602. doi: 10.1038/s41568-019-0186-9

11. Riley R, June C, Langer R, et al. Delivery technologies for cancer immunotherapy. *Nat Rev Drug Discov.* 2019; 18: 175-196. doi: 10.1038/s41573-018-0006-z

12. Veronese F, Pasut G. PEGylation, successful approach to drug delivery. *Drug Discov Today.* 2005; 10(21): 1451-8. doi: 10.1016/S1359-6446(05)03575-0

13. Lobouta H, Gomez-Garcia J, Sarsons C, et al. Surface-grafted polyethylene glycol conformation impacts the transport of PEG-functionalized liposomes through a tumor extracellular matrix model. *RCS Adv.* 2018; 14: 7697-7708. doi: 10.1039/C7RA13438J

14. Cruje C, Chithrani D. Polyethylene Glycol Density and Length Affects Nanoparticle Uptake by Cancer Cells. *J Nanomed Res.* 2014; 1(1): 00006. doi: 10.15406/jnmr.2014.01.00006

15. Perry J, Reuter K, Kai M, et al. PEGylated PRINT Nanoparticles: The Impact of PEG Density on Protein Binding, Macrophage Association, Biodistribution, and Pharmacokinetics. *Nano Lett.* 2012; 12(10): 5304-5310. doi: 10.1021/nl302638g

16. Barber, G. STING: infection, inflammation and cancer. *Nat Rev Immunol.* 2015; 15: 760-770. doi: 10.1038/nri3921

17. Su T, Zhang Y, Valerie K, et al. STING activation in cancer immunotherapy. *Theranostics.* 2019; 9(25): 7759-7771. doi: 10.7150/thno.37574

18. Alothman Z. A Review: Fundamental Aspects of Silicate Mesoporous Materials. *Materials.* 2012; 5(12): 2874-2902. doi: 10.3390/ma5122874

19. Wojnilowicz M, Glab A, Bertucci A, et al. Super-resolution Imaging of Proton Sponge-Triggered Rupture of Endosomes and Cytosolic Release of Small Interfering RNA. *ACS Nano.* 2019; 13(1): 187-202. doi: 10.1021/acsnano.8b05151

20. Curtis K, Miller D, Millard P, et al. Unusual Salt and pH Induced Changes in Polyethylenimine Solutions. *PLoS One.* 2016; 11(9). doi: 10.1371/journal.pone.0158147

21. Pages F, Mlecnik B, Marliot F, et al. International validation of the consensus Immunoscore for the classification of colon cancer: a prognostic and accuracy study. *Lancet.* 2018; 391(10135): 2128-2139. doi: 10.1016/s0140-6736(18)30789-x

22. Bagley S, O'Rourke D. Clinical investigation of CAR T cells for solid tumors: Lessons learned and future directions. *Pharmacol Therapeut.* 2020; 205(107419). doi: 10.1016/j.pharmthera.2019.107419.

23. Ottaviano M, De Placido S, Antonio Ascierto P. Recent success and limitations of immune checkpoint inhibitors for cancer: a lesson from melanoma. *Virchows Archiv.* 2019; 474: 421-432. doi: 10.1007/s00428-019-02538-4

24. Fitzgerald-Bocarsly P, Feng D. The role of type I interferon production by dendritic cells in host defense. *Biochimie*. 2007; 89(6-7): 843-855. doi: 10.1016/j.biochi.2007.04.018

25. Marcus A, Mao A, Lensink-Vasan M, et al. Tumor-derived cGAMP triggers a STING-mediated interferon response in non-tumor cells to activate the NK cell response. *Immunity.* 2018; 49(4): 754-763. doi: 10.1016/j.immuni.2018.09.016

26. Simmons D, Wearsch P, Canaday D, et al. Type I interferon drives a distinctive dendritic cell maturation phenotype that allows continued class II MHC synthesis and antigen processing. *J Immunol.* 2012; 188(7): 3116-26. doi: 10.4049/jimmunol.1101313

27. Fuertes M, Kacha A, Kline J, et al. Host type I IFN signals are required for antitumor $CD8^+$ T cell responses through $CD8\alpha^+$ dendritic cells. *J Exp Med.* 2011; 208(10): 2005-2016. doi: 10.1084/jem.20101159

28. Keun Kim Y, Shin JS, Nahm M. NOD-Like Receptors in Infection, Immunity, and Diseases. *Yonsei Med J.* 2016; 57(1): 5-14. doi: 10.3349/ymj.2016.57.1.5

29. Urban-Wojciuk Z, Khan M, Oyler B, et al. The Role of TLRs in Anti-cancer Immunity and Tumor Rejection. *Front Immunol.* 2019; 10(2388). doi: 10.3389/fimmu.2019.02388

30. Jahrsdorfer B, Weiner G. CpG oligodeoxynucleotides as immunotherapy in cancer. *Update Cancer Ther.* 2008; 3(1): 27-32. doi: 10.1016/j.uct.2007.11.003

31. Turan O, Bielecki P, Perera V, et al. Delivery of drugs into brain tumors using multicomponent silica nanoparticles. *Nanoscale*. 2019;11(24):11910-11921. doi:10.1039/c9nr02876e

32. Turan O, Bielecki PA, Perera V, et al. Treatment of Glioblastoma Using Multicomponent Silica Nanoparticles. *Adv Ther*. 2019;2(11):1900118. doi:10.1002/adtp.201900118

33. Turan O, Bielecki P, Tong K, et al. Effect of Dose and Selection of Two Different Ligands on the Deposition and Antitumor Efficacy of Targeted Nanoparticles in Brain Tumors. *Mol Pharm*. 2019;16(10):4352-4360. doi:10.1021/acs.molpharmaceut.9b00693